Numerical Simulation of the Cosmic Microwave Background Formation

William Eivik Olsen*
University of Oslo - Department of Physics

(Dated: May 28, 2021)

We simulate the formation of the cosmic microwave background for the ΛCDM model of cosmology. We do so by calculating the evolution of the background, including recombination. We then add linear perturbations to the background metric and energy contents with initial conditions predicted by inflation. The density perturbations are finally used to calculate the CMB and matter spectra through line-of-sight integration. Our results are close to agreement with observational data, but have some deviations. The deviations are expected as we make some simplifying assumptions in the calculations: We have excluded the effects of neutrinos, helium, reionization and polarization.

INTRODUCTION

The Cosmic Microwave Background (CMB) provides the most direct observational link to the physics of the early Universe: The CMB photons we observe today were emitted roughly 380,000 years after the Big Bang. It therefore serves as the most important observable of cosmology.

The black body spectrum of the CMB is the most perfect black body to ever be observed in nature [4]. There are however some small deviations from the black body, referred to as *anisotropies*. These anisotropies are thought to be related to density perturbations in the primordial plasma, responsible for the structure and evolution of the Universe as we observe it today. Through our models of cosmology we can make predictions of how and why the anisotropies formed. This can be tested against the observed anisotropies.

In this paper we intend to do exactly that: Make a numerical simulation of the CMB formation. Our paper will be divided into four milestones:

I Background cosmology: We simulate the evolution of the uniform background of the Universe. This provides the expansion history and the evolution of the energy contents.

II Recombination: We simulate the evolution of the plasma of photons, electrons and protons in the early Universe. This provides the time of last scattering, after which CMB photons could move freely.

III Perturbations: We add some small initial perturbations to the metric and energy contents and simulate their evolution.

IV CMB and matter power spectra: We calculate the CMB and matter power spectra using the evolution of the perturbations.

* Code repository: https://github.com/williameivikolsen/AST5220

MILESTONE I: BACKGROUND COSMOLOGY

Introduction

To begin with we will consider the evolution of the uniform background of the Universe. Our goal will be to calculate the evolution of the Hubble parameter, the energy content and the conformal time. We will model the Universe using the ΛCDM model, assuming the Universe to be flat.

Theory

The Friedmann equation for the ΛCDM Model can be written as

$$H = H_0\sqrt{(\Omega_{b0}+\Omega_{\text{CDM0}})a^{-3} + (\Omega_{\gamma 0}+\Omega_{\nu 0})a^{-4} + \Omega_{k0}a^{-2} + \Omega_{\Lambda 0}}, \quad (1)$$

where $H \equiv \dot{a}/a$ is the Hubble parameter and Ω_{b0}, Ω_{CDM0}, $\Omega_{\gamma 0}$, $\Omega_{\nu 0}$, Ω_{k0} and $\Omega_{\Lambda 0}$ are the present day relative densities of baryonic matter, dark matter, radiation, neutrinos, curvature and dark energy, respectively. Note that the relative curvature density $\Omega_{k0} = -\frac{kc^2}{H_0^2}$ acts as if it were a normal matter fluid with equation of state $\omega \equiv P/\rho = -1/3$.

We also define a function $\mathcal{H} \equiv aH$. From (1) it then follows that

$$\frac{\mathrm{d}\mathcal{H}}{\mathrm{d}x} = \frac{H_0^2}{2\mathcal{H}}\big(2\Omega_{\Lambda 0}e^{2x} - (\Omega_{b0}+\Omega_{CDM0})e^{-x} - 2(\Omega_{\gamma 0}+\Omega_{\nu 0})e^{-2x}\big), \quad (2)$$

$$\frac{\mathrm{d}^2\mathcal{H}}{\mathrm{d}x^2} = \frac{H_0^2}{2\mathcal{H}}\big(4\Omega_{\Lambda 0}e^{2x} + (\Omega_{b0}+\Omega_{CDM0})e^{-x} + 4(\Omega_{\gamma 0}+\Omega_{\nu 0})e^{-2x}\big) - \frac{H_0^4}{4\mathcal{H}^3}\big(2\Omega_{\Lambda 0}e^{2x} - (\Omega_{b0}+\Omega_{CDM0})e^{-x} - 2(\Omega_{\gamma 0}+\Omega_{\nu 0})e^{-2x}\big)^2. \quad (3)$$

The time evolution of the densities is given by

$$\dot{\rho} + 3H(\rho + P) = 0. \quad (4)$$

The solution can be written in terms of the equation of state as

$$\rho \propto a^{-3(1+\omega)}. \tag{5}$$

The equation of state is $\omega = 0$ for cold dark matter and baryons, $\omega = 1/3$ for relativistic matter and $\omega = -1$ for the cosmological constant. This gives

$$\begin{aligned}\rho_{\mathrm{CDM}} &= \rho_{\mathrm{CDM},0} a^{-3}\\ \rho_b &= \rho_{b,0} a^{-3}\\ \rho_\gamma &= \rho_{\gamma,0} a^{-4}\\ \rho_\nu &= \rho_{\nu,0} a^{-4}\\ \rho_\Lambda &= \rho_{\Lambda,0},\end{aligned}$$

where subscript 0 denotes present day values. The relative densities $\Omega_X(a) = \rho_X/\rho_c$ can be written

$$\begin{aligned}\Omega_k(a) &= \frac{\Omega_{k0}}{a^2 H(a)^2/H_0^2},\\ \Omega_{\mathrm{CDM}}(a) &= \frac{\Omega_{\mathrm{CDM0}}}{a^3 H(a)^2/H_0^2},\\ \Omega_b(a) &= \frac{\Omega_{b0}}{a^3 H(a)^2/H_0^2},\\ \Omega_\gamma(a) &= \frac{\Omega_{\gamma 0}}{a^4 H(a)^2/H_0^2},\\ \Omega_\nu(a) &= \frac{\Omega_{\nu 0}}{a^4 H(a)^2/H_0^2},\\ \Omega_\Lambda(a) &= \frac{\Omega_{\Lambda 0}}{H(a)^2/H_0^2}.\end{aligned}$$

The relative densities of the relativistic matter can be calculated from the CMB temperature through

$$\begin{aligned}\Omega_{\gamma 0} &= 2 \cdot \frac{\pi^2}{30} \frac{(k_b T_{\mathrm{CMB0}})^4}{\hbar^3 c^5} \cdot \frac{8\pi G}{3H_0^2},\\ \Omega_{\nu 0} &= N_{\mathrm{eff}} \cdot \frac{7}{8} \cdot \left(\frac{4}{11}\right)^{4/3} \Omega_{\gamma 0},\end{aligned}$$

where N_{eff} is the effective number of massless neutrinos.

The relativistic matter is expected to dominate the early Universe as $a \to 0$, while dark energy is expected to dominate the Universe in the distant future as $a \to \infty$. Assuming the Universe to be dominated by a fluid with equation of state ω, the Friedmann equation takes the form

$$H = H_0 a^{-\frac{3}{2}(1+\omega)}.$$

This implies that $\mathcal{H}$ will satisfy

$$\begin{aligned}\frac{1}{\mathcal{H}}\frac{\mathrm{d}\mathcal{H}}{\mathrm{d}x} &= -\frac{1+3\omega}{2},\\ \frac{1}{\mathcal{H}}\frac{\mathrm{d}^2\mathcal{H}}{\mathrm{d}x^2} &= \frac{(1+3\omega)^2}{4}.\end{aligned}$$

We therefore expect that as relativistic matter dominates in the early Universe, $\frac{1}{\mathcal{H}}\frac{\mathrm{d}\mathcal{H}}{\mathrm{d}x} = -1$ and $\frac{1}{\mathcal{H}}\frac{\mathrm{d}^2\mathcal{H}}{\mathrm{d}x^2} = 1$. Likewise we expect that when dark energy dominates in the distant future, $\frac{1}{\mathcal{H}}\frac{\mathrm{d}\mathcal{H}}{\mathrm{d}x} = 1$ and $\frac{1}{\mathcal{H}}\frac{\mathrm{d}^2\mathcal{H}}{\mathrm{d}x^2} = 1$.

The amount of matter (baryons and dark matter) is equal to the amount of radiation (photons and neutrinos) when $a = a_\gamma$, where

$$a_\gamma = \frac{\Omega_{\gamma 0} + \Omega_{\nu 0}}{\Omega_{b0} + \Omega_{CDM0}}. \tag{6}$$

Likewise, the amount of matter is equal to the amount of dark energy when $a = a_\Lambda$, where

$$a_\Lambda = \sqrt[3]{\frac{\Omega_{b0} + \Omega_{CDM0}}{\Omega_{\Lambda 0}}}. \tag{7}$$

The Universe will start to accelerate at the matter-dark energy equality.

The comoving horizon is the distance light may have travelled since the Big Bang. Since it is monotonically increasing it can be used as a time variable. We refer to this time variable as the conformal time η. The conformal time can be calculated through the differential equation

$$\frac{d\eta}{dx} = \frac{c}{\mathcal{H}}, \tag{8}$$

where $x \equiv \log a$ and $\mathcal{H} \equiv aH$. The initial condition of the equation is $\eta(-\infty) = 0$.

The age of the universe t can similarly be computed by solving the differential equation

$$\frac{dt}{dx} = \frac{1}{H}, \tag{9}$$

and evaluating it at $x = 0$. The initial condition is $t(x_{\mathrm{start}}) = \frac{1}{2H(x_{\mathrm{start}})}$.

In the radiation dominated era in the early Universe we have that $H^2 = H_0^2 a^{-4}$. Equation (8) then takes the form

$$\frac{\mathrm{d}\eta}{\mathrm{d}x} = \frac{c}{\mathcal{H}} = \frac{c}{aH} = \frac{c}{aH_0 a^{-2}} = \frac{c}{H_0} a = \frac{c}{H_0} e^x,$$

giving the solution

$$\eta = \frac{c}{H_0} e^x = \frac{c}{\mathcal{H}}.$$

We therefore expect that

$$\frac{\eta \mathcal{H}}{c} = 1 \tag{10}$$

in the early Universe.

The luminosity distance d_L is related to the conformal time η by

$$d_L = \frac{\eta_0 - \eta}{a} \tag{11}$$

where η_0 is the present day value of η (evaluated at $a = 1$).

The redshift z is defined as

$$1 + z \equiv \frac{1}{a}. \tag{12}$$

Implementation Details

The background evolution was calculated numerically using a numerical solver that takes in h, Ω_{b0}, Ω_{CDM0}, Ω_{k0}, N_{eff} and T_{CMB0} as paramters. We assume space to be flat so that $\Omega_{k0} = 0$. We only consider the simplified model where there are no neutrinos, $N_{eff} = 0$. For the other parameters we use the best-fit values from the Planck 2018 data [1]:

$$\begin{aligned} h &= 0.67 \\ \Omega_{b0} &= 0.05 \\ \Omega_{CDM0} &= 0.267 \\ T_{CMB0} &= 2.7255 \text{ K} \end{aligned}$$

The differential equations (8) and (9) were solved using the Runge-Kutta 4 method. We made cubic splines of the solutions.

The luminosity distance was calculated through (11) and compared to type Ia supernova observations [2].

Results

The age of the Universe t, the matter-radiation equality a_γ and the matter-dark energy equality a_Λ were found to be

$$\begin{aligned} t &= 13.8508 \times 10^9 \text{ years}, \\ a_\gamma &= 1.74 \times 10^{-4}, \\ a_\Lambda &= 7.74 \times 10^{-1}. \end{aligned}$$

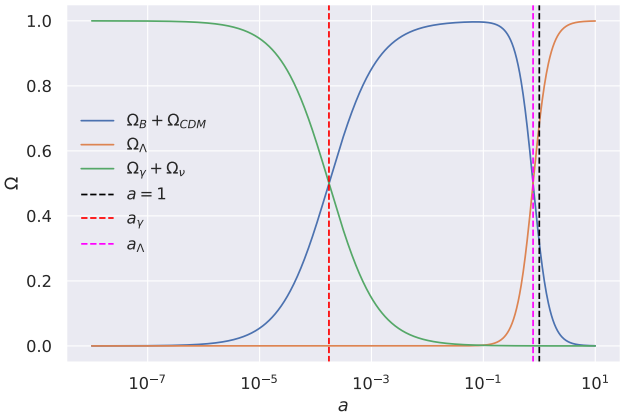

Figure 1. Evolution of the relative densities. Radiation-matter equality is marked by a_γ. Matter-dark energy equality is marked by a_Λ.

Discussion

In figure 1 we see that our expectation that the Universe was dominated by relativistic particles in the beginning is indeed correct. The baryons and dark matter then takes over as the dominating component at $a_\gamma = 1.74 \times 10^{-4}$. Finally, just before today, the cosmological constant takes over as the largest quantity at $a_\Lambda = 7.74 \times 10^{-1}$. The cosmological constant then goes over to dominate the energy density of the Universe, as we also expected.

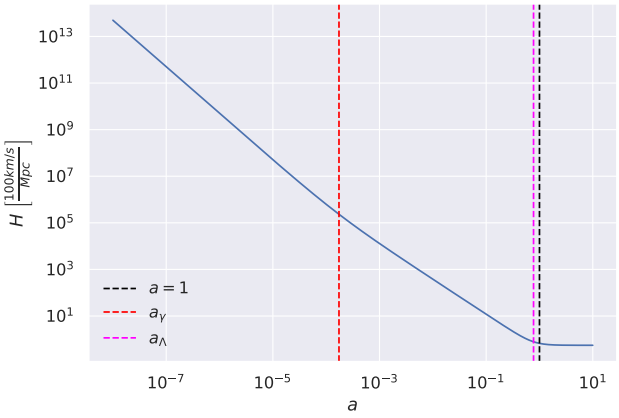

Figure 2. Evolution of the Hubble parameter H. Radiation-matter equality is marked by a_γ. Matter-dark energy equality is marked by a_Λ.

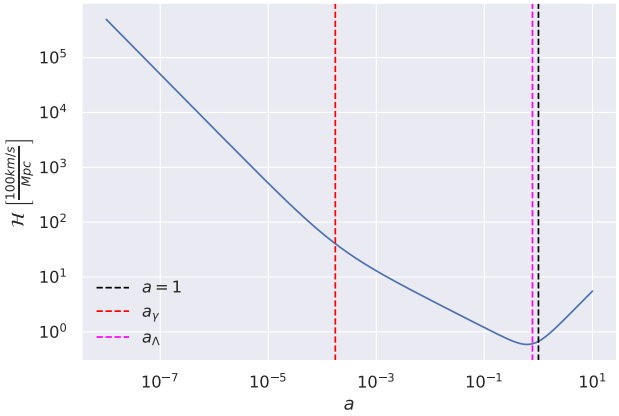

Figure 3. Evolution of $\mathcal{H}$. Radiation-matter equality is marked by a_γ. Matter-dark energy equality is marked by a_Λ.

In figure 2 we see how the Hubble parameter changes as the Universe expands. We see that it decreases monotonically until the matter-dark energy equality. Here it seems to stabilize to a constant value. In figure 3 we see that at the same point $\mathcal{H}$, which is equivalent to $\dot{a}$, is at a minimum after which it increases: The Universe begins accelerating, as we expected when the cosmological constant took over as the dominating form of energy.

We also had some expectations as to how the derivative and second derivative of $\mathcal{H}$ would evolve during the expansion. In figure 4 we see that these expectations

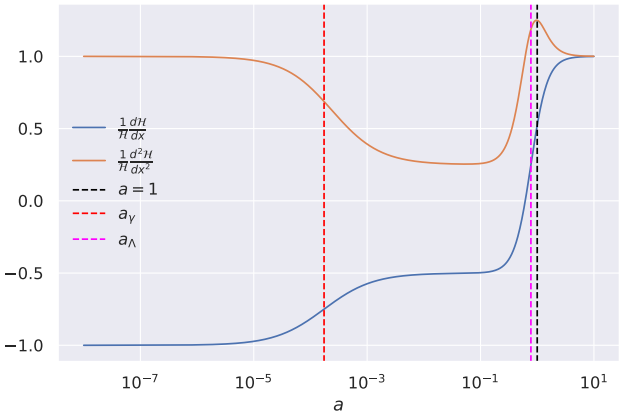

Figure 4. Evolution of $\frac{1}{\mathcal{H}}\frac{\mathrm{d}H}{\mathrm{d}x}$ and $\frac{1}{\mathcal{H}}\frac{\mathrm{d}^2H}{\mathrm{d}x^2}$. Radiation-matter equality is marked by a_γ. Matter-dark energy equality is marked by a_Λ.

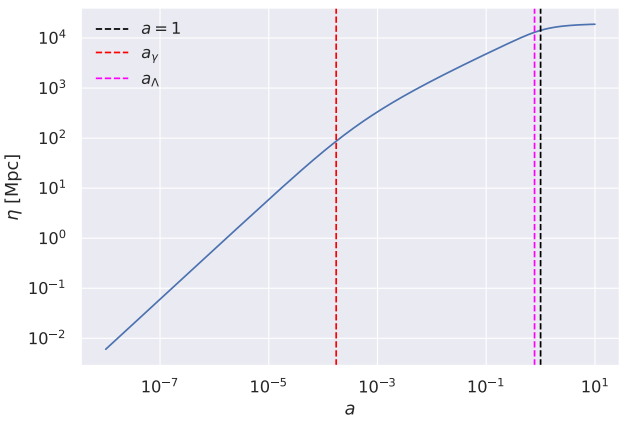

Figure 5. Evolution of η. Radiation-matter equality is marked by a_γ. Matter-dark energy equality is marked by a_Λ.

were indeed satisfied: In the radiation dominated era at the beginning, $\frac{1}{\mathcal{H}}\frac{\mathrm{d}\mathcal{H}}{\mathrm{d}x} = -1$ and $\frac{1}{\mathcal{H}}\frac{\mathrm{d}^2\mathcal{H}}{\mathrm{d}x^2} = 1$. In the distant future when the cosmological constant dominates, $\frac{1}{\mathcal{H}}\frac{\mathrm{d}\mathcal{H}}{\mathrm{d}x} = 1$ and $\frac{1}{\mathcal{H}}\frac{\mathrm{d}^2\mathcal{H}}{\mathrm{d}x^2} = 1$.

The conformal time η increases monotonically over the entire evolution of the Universe, however much slower after the matter-dark energy equality. We see that our expectation that $\eta\mathcal{H}/c = 1$ in the early Universe is fulfilled in 6.

Finally, we see that our predicted luminosity distance fits well with the observed type Ia supernova in figure 7.

MILESTONE II: RECOMBINATION

Introduction

The early Universe was filled with a plasma of free electrons and protons. They carry a charge and therefore interact with photons. If we want to understand the evolution of the photons that make the CMB we should therefore begin with the evolution of the early plasma.

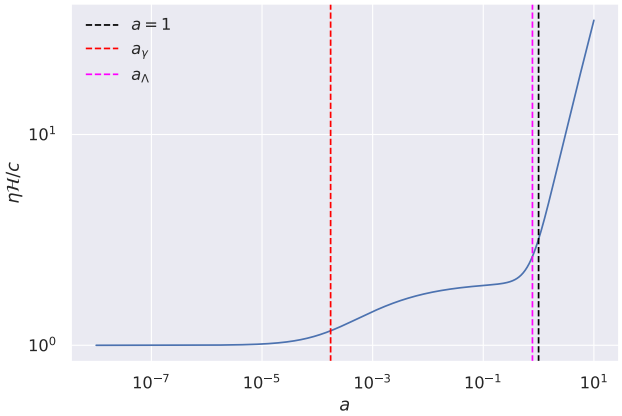

Figure 6. Evolution of $\eta\mathcal{H}/c$. Radiation-matter equality is marked by a_γ. Matter-dark energy equality is marked by a_Λ.

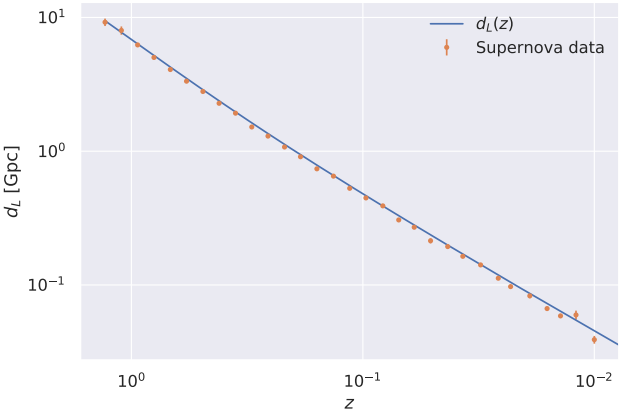

Figure 7. Computed luminosity distance d_L and data.

As the Universe expands we expect the temperature of the plasma to decrease. We also expect that at some point, when the temperature of the plasma is lower than the ionization energy of hydrogen, the electrons and protons can come together and form neutral hydrogen, allowing the photons to move freely. This is what we call recombination.

The interaction of photons with electrons and protons happens through the process of Thomson scattering. The Thomson cross section of protons is much smaller than that of electrons due to the proton having a much higher mass than the electron, making the proton interaction negligible. We therefore wish to study how the number of free electrons evolve with time. Then we can quantify the absorption of photons in the plasma by the optical depth, which is related to the number of free electrons.

Our goal with this milestone will be to compute the optical depth $\tau(x)$. We will also compute the visibility

function $\tilde{g}(x)$, which represents the probability that a CMB photon observed today was last scattered at the time x. We make the simplifying assumption that all baryons are protons.

Theory

An observer a distance x away from a source emitting an intensity I_0 through a medium will observe an intensity $I = I_0 e^{-\tau(x)}$ where $\tau(x)$ is the optical depth. In cosmology the main absorption is Thomson scattering of photons off free electrons. The optical depth is related to the Thomson scattering cross section σ_T by

$$\frac{\mathrm{d}\tau}{\mathrm{d}x} = -\frac{cn_e\sigma_T}{H}, \tag{13}$$

where n_e is the electron number density. The surface of last scattering is defined to be the time $x_{\text{decoupling}}$ when $\tau(x_{\text{decoupling}}) = 1$. From the optical depth the visibility function $\tilde{g}(x)$ can be computed:

$$\tilde{g}(x) = -\frac{\mathrm{d}\tau}{\mathrm{d}x} e^{-\tau(x)}. \tag{14}$$

In order to compute the optical depth and visibility function we must first compute the electron number density n_e as a function of the scale factor. We define the fractional electron density as $X_e = n_e/n_H$ where n_H is the proton number density. Given the assumption that all baryons are protons, we have

$$n_H = \frac{\Omega_{b0}\rho_{c0}}{m_H a^3} \tag{15}$$

where m_H is the hydrogen mass.

The fractional electron density can be computed by the Peebles equation

$$\frac{dX_e}{dx} = \frac{C_r(T_b)}{H}\left[\beta(T_b)(1-X_e) - n_H\alpha^{(2)}(T_b)X_e^2\right], \tag{16}$$

where

$$\begin{aligned}
C_r(T_b) &= \frac{\Lambda_{2s\to 1s} + \Lambda_\alpha}{\Lambda_{2s\to 1s} + \Lambda_\alpha + \beta^{(2)}(T_b)},\\
\Lambda_{2s\to 1s} &= 8.227\text{s}^{-1},\\
\Lambda_\alpha &= H\frac{(3\epsilon_0/(\hbar c))^3}{(8\pi)^2 n_{1s}},\\
n_{1s} &= (1-X_e)n_H,\\
n_H &= \frac{3H_0^2\Omega_{b0}}{8\pi G m_H a^3},\\
\beta^{(2)}(T_b) &= \beta(T_b)e^{3\epsilon_0/(4k_BT_b)},\\
\beta(T_b) &= \alpha^{(2)}(T_b)\left(\frac{m_e k_B T_b}{2\pi\hbar^2}\right)^{3/2} e^{-\epsilon_0/(k_BT_b)},\\
\alpha^{(2)}(T_b) &= \frac{64\pi}{\sqrt{27\pi}}\frac{\alpha^2\hbar^2}{m_e^2 c}\sqrt{\frac{\epsilon_0}{k_BT_b}}\phi_2(T_b),\\
\phi_2(T_b) &= 0.448\ln\left(\frac{\epsilon_0}{k_BT_b}\right).
\end{aligned}$$

Here $\alpha \simeq \frac{1}{137.0359992}$ is the fine-structure constant, T_b is the baryon temperature and $\epsilon_0 = 13.6$ eV is the ionization energy of hydrogen.

The Peebles equation is an excellent approximation. It is however numerically unstable for $X_e \approx 1$. In this regime a simpler approximation can be made, namely the Saha equation:

$$\frac{X_e^2}{1-X_e} = \frac{1}{n_H}\left(\frac{m_e k_B T_b}{2\pi\hbar^2}\right)^{3/2} e^{-\epsilon_0/(k_BT_b)}. \tag{17}$$

The Saha equation is made from the assumption that the reaction

$$e^- + p^+ \rightleftharpoons H + \gamma$$

is at equilibrium.

We make the assumption that the baryon and photon temperature is the same:

$$T_b = T_\gamma = \frac{T_{CMB0}}{a}. \tag{18}$$

Implementation Details

The Peebles and Saha equations (16) and (17) were implemented to calculate the fractional electron density numerically. For $X_e \geq 0.99$ the Saha equation was used, while the Peebles equation was used for the remaining values. The Peebles equation was solved using the Runge-Kutta 4 method. We made a cubic spline of the solution $X_e(x)$. From this we computed the electron number density through $n_e = n_H X_e$, using equation (15) for n_H.

Differential equation (13) was then solved for τ using the Runge-Kutta 4 method. We made a cubic spline of the solution $\tau(x)$ and used this to calculate the visibility function $\tilde{g}(x)$ through equation (14).

Note that we simplified our computations by not taking reionization into account.

Results

The surface of last scattering was found to be

$$\begin{aligned}
x_{\text{decoupling}} &= -6.99,\\
z_{\text{decoupling}} &= 1081.3.
\end{aligned}$$

The halfway-point of recombination at which $X_e = 0.5$ was

$$\begin{aligned}
x_{\text{rec}} &= -7.16,\\
z_{\text{rec}} &= 1290.8.
\end{aligned}$$

The freeze-out abundance of electrons was

$$X_e(x=0) = 1.99\times 10^{-4}.$$

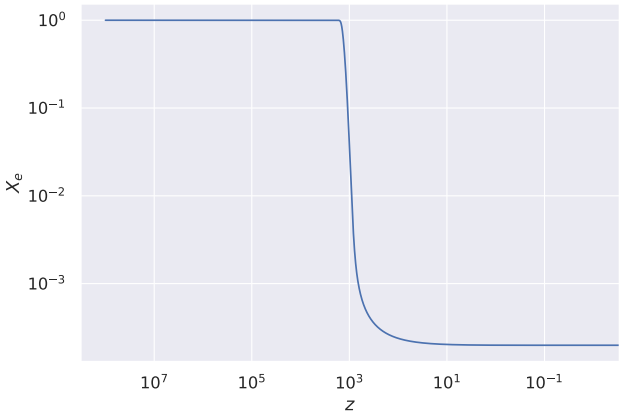

Figure 8. Fractional electron density as function of redshift z. The Saha equation (17) was used to calculate the values for $X_e \geq 0.99$, while the Peebles equation (16) was used to calculate the remaining values.

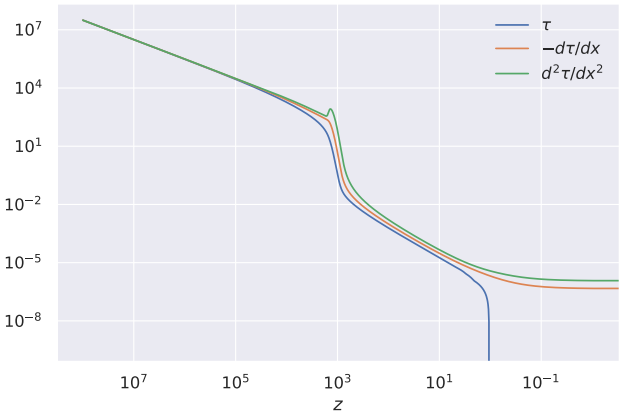

Figure 9. Optical depth τ and its first and second derivatives $\frac{\mathrm{d}\tau}{\mathrm{d}x}$ and $\frac{\mathrm{d}^2\tau}{\mathrm{d}x^2}$ as function of redshift z.

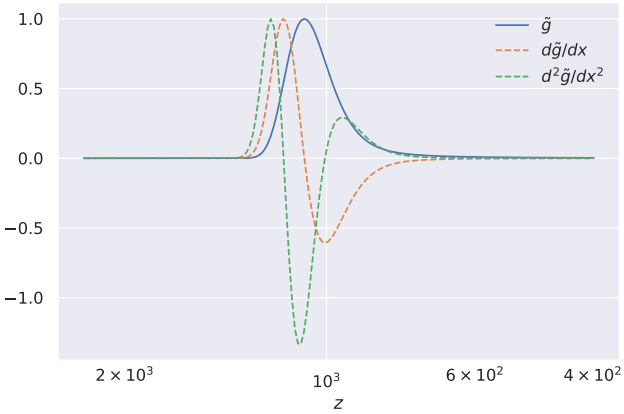

Figure 10. Visibility function $\tilde{g}$ and its derivatives as function of redshift z. Note that the functions are scaled down by their maximal values $\tilde{g}_{max} = 4.9$, $\tilde{g}'_{max} = 50.4$, $\tilde{g}''_{max} = 728.0$.

Discussion

The evolution of the fractional electron density is shown in figure 8. We see that $X_e \approx 1$ in the early Universe, before starting a rapid decrease during recombination around $z \approx 10^3$. The halfway-point of recombination $z_{\text{rec}} = 1290.8$ was lower than that predicted by the Saha equation (17): Inserting $X_e = 0.5$ gives the solution $z = 1379.4$. This is because the equilibrium assumption of the Saha equation fails to hold when the abundance of free electrons and protons gets small. At this point the low probability of electrons and protons meeting makes the reaction inefficient, causing the reaction to drop out of equilibrium and eventually freeze out around $z_{\text{decoupling}} = 1081.3$. After this time the fractional electron density stays constant (since we do not consider reionization) at the freeze-out abundance of today, $X_e(x = 0) = 1.99 \times 10^{-4}$.

The baryon temperature at the freeze-out is $T_b = 2950$ K, corresponding to an energy of 0.25 eV. This energy is lower than the hydrogen ionization energy ϵ_0. This is because when neutral hydrogen is formed, it gets ionized instantaneously because of the high number of photons compared to the number of baryons, causing a delay in recombination.

In figure 9 we see that the optical depth goes from being extremely high to a rapid descent as the number of free electrons falls around $z_{\text{decoupling}}$. The lowered number of free electrons allows photons to travel freely, as expected. For this reason the visiblity function $\tilde{g}$, shown in figure 10, has a peak at $z_{\text{decoupling}} = 1081.3$, meaning that a CMB photon observed today was most likely last scattered at this moment. The low number of free electrons for $z < z_{\text{decoupling}}$ makes it unlikely that a CMB photon was scattered at a later time, causing the visibility function to quickly decrease to 0.

MILESTONE III: PERTURBATIONS

Introduction

For the time being we have only considered the Universe as a smooth fluid. This works well as an approximation, but the Universe we know and love is obviously not a homogeneous fluid: It is filled with galaxies, stars, planets, cats and dogs. To model this we wish to add some small perturbations to the Einstein and Boltzmann equations. The main goal of this milestone is to compute the evolution of these perturbations in Fourier space. Note that we still assume a neutrino-free Universe.

Theory

We need to add perturbations to both the distribution functions f_i of the matter we consider and to the metric.

For the metric we will have to choose a gauge. This will be the Newtonian gauge:

$$\mathrm{d}s^2 = -(1+2\Psi)dt^2 + a^2(1+2\Phi)(dx^2+dy^2+dz^2), \quad (19)$$

where Φ and Ψ are functions of space and time.

We define the photon perturbations Θ as the perturbation in the local photon temperature T:

$$\Theta(t, \mathbf{x}, \hat{\mathbf{p}}) = \frac{\delta T}{\overline{T}}. \quad (20)$$

Note that Θ only depends on the momentum direction $\hat{\mathbf{p}}$ and not the momentum p. This is because the only relevant interaction for photons is Compton scattering, which to first order only changes direction and not momentum of photons. In Fourier space we have $\Theta = \Theta(t, k, \mu)$, where $\mathbf{k}$ is the wave vector, $k = |\mathbf{k}|$ and $\mu = \hat{\mathbf{p}} \cdot \mathbf{k}/k$. We make a multipole expansion of Θ:

$$\Theta(t, k, \mu) = \sum \frac{2\ell+1}{i^\ell} \Theta_\ell(t, k) P_\ell(\mu), \quad (21)$$

where P_ℓ are the Legendre polynomials and the photon multiples Θ_ℓ are given by

$$\Theta_\ell = \frac{i^\ell}{2} \int_{-1}^{1} \Theta(t, k, \mu) P_\ell(\mu) d\mu. \quad (22)$$

Having perturbed the distribution functions $f_i = \overline{f}_i + \delta f_i$ we can evaluate the Boltzmann equation $\frac{\mathrm{d}f_i}{\mathrm{d}t} = C_i$ for each of the quantities. This can be used to find the perturbed energy momentum tensor $\delta T_{\mu\nu}$. Using the metric (19) we can set up the perturbed Einstein equations $\delta G_{\mu\nu} = 8\pi G \delta T_{\mu\nu}$. Taken together this leaves us with the Einstein-Boltzmann equations, a closed system of differential equations for the metric perturbation and density and velocity of the energy contents. In Fourier space they are given by

$$\begin{aligned}
\Phi' &= \Psi - \frac{c^2k^2}{3\mathcal{H}^2}\Phi + \frac{H_0^2}{2\mathcal{H}^2}\big[\Omega_{\mathrm{CDM}0} a^{-1} \delta_{\mathrm{CDM}} \\
&\qquad + \Omega_{b0} a^{-1} \delta_b + 4\Omega_{\gamma 0} a^{-2} \Theta_0\big], \\
\Psi &= -\Phi - \frac{12H_0^2}{c^2k^2a^2}\Omega_{\gamma 0}\Theta_2, \\
\delta'_{\mathrm{CDM}} &= \frac{ck}{\mathcal{H}} v_{\mathrm{CDM}} - 3\Phi', \\
v'_{\mathrm{CDM}} &= -v_{\mathrm{CDM}} - \frac{ck}{\mathcal{H}}\Psi, \\
\delta'_b &= \frac{ck}{\mathcal{H}} v_b - 3\Phi', \\
v'_b &= -v_b - \frac{ck}{\mathcal{H}}\Psi + \tau' R(3\Theta_1 + v_b), \\
\Theta'_0 &= -\frac{ck}{\mathcal{H}}\Theta_1 - \Phi', \\
\Theta'_1 &= \frac{ck}{3\mathcal{H}}\Theta_0 - \frac{2ck}{3\mathcal{H}}\Theta_2 + \frac{ck}{3\mathcal{H}}\Psi + \tau'\left[\Theta_1 + \frac{1}{3}v_b\right], \\
\Theta'_\ell &= \frac{\ell ck}{(2\ell+1)\mathcal{H}}\Theta_{\ell-1} - \frac{(\ell+1)ck}{(2\ell+1)\mathcal{H}}\Theta_{\ell+1} \\
&\qquad + \tau'\left[\Theta_\ell - \frac{1}{10}\Theta_2\delta_{\ell,2}\right], \qquad 2 \le \ell < \ell_{\max} \\
\Theta'_\ell &= \frac{ck}{\mathcal{H}}\Theta_{\ell-1} - c\frac{\ell+1}{\mathcal{H}\eta(x)}\Theta_\ell + \tau'\Theta_\ell, \qquad \ell = \ell_{\max}.
\end{aligned}$$

Here δ_b and v_b are the density perturbation and velocity of baryons and δ_{CDM} and v_{CDM} the same of dark matter. The parameter $R = \frac{4\Omega_{\gamma 0}}{3\Omega_{b0}a}$. The initial conditions can be derived from inflation theory:

$$\begin{aligned}
\Psi &= -\frac{2}{3} \\
\Phi &= -\Psi \\
\delta_{\mathrm{CDM}} &= \delta_b = -\frac{3}{2}\Psi \\
v_{\mathrm{CDM}} &= v_b = -\frac{ck}{2\mathcal{H}}\Psi \\
\Theta_0 &= -\frac{1}{2}\Psi \\
\Theta_1 &= +\frac{ck}{6\mathcal{H}}\Psi \\
\Theta_2 &= -\frac{4ck}{9\mathcal{H}\tau'}\Theta_1, \\
\Theta_\ell &= -\frac{\ell}{2\ell+1}\frac{ck}{\mathcal{H}\tau'}\Theta_{\ell-1}.
\end{aligned}$$

At early times the optical depth τ is very high. This causes electrons to only be affected by the temperature fluctuations of nearby electrons. Since the full system is in thermodynamic equilibrium there will therefore only be smooth temperature fluctuations. We call this regime *tight coupling*. The Einstein-Boltzmann equations are numerically unstable during tight coupling. In order to solve this problem we will approximate the quantity

$(3\Theta_1 + v_b)$, which is very small early on. The approximation is the following:

$$q = \Bigg[-[(1-R)\tau' + (1+R)\tau''](3\Theta_1 + v_b) - \frac{ck}{\mathcal{H}}\Psi + (1 - \frac{\mathcal{H}'}{\mathcal{H}})\frac{ck}{\mathcal{H}}(-\Theta_0 + 2\Theta_2) - \frac{ck}{\mathcal{H}}\Theta_0' \Bigg] \Bigg/ \left[(1+R)\tau' + \frac{\mathcal{H}'}{\mathcal{H}} - 1\right],$$

$$v_b' = \frac{1}{1+R}\left[-v_b - \frac{ck}{\mathcal{H}}\Psi + R(q + \frac{ck}{\mathcal{H}}(-\Theta_0 + 2\Theta_2) - \frac{ck}{\mathcal{H}}\Psi)\right],$$

$$\Theta_1' = \frac{1}{3}(q - v_b').$$

Note that during tight coupling the only relevant photon multipoles are the monopole Θ_0, the dipole Θ_1 and the quadrupole Θ_2. The Einstein-Boltzmann equations can therefore be solved as they would otherwise, except from using the approximation for Θ_1' and ignoring all multipoles with $\ell > 2$.

Tight coupling is valid at all times before recombination as long as

$$\left|\frac{\mathrm{d}\tau}{\mathrm{d}x}\right| < 10 \cdot \max(1, ck/\mathcal{H}). \tag{23}$$

Implementation Details

The Einstein-Boltzmann equations were solved numerically. During tight coupling we only included $\ell \leq 2$ for the photon multipoles Θ_ℓ, with the tight coupling approximation used for Θ_1'. After tight coupling the full Boltzmann-Einstein equations were used, including multipoles Θ_ℓ with $\ell \leq 7$.

Results and Discussion

In figure 11 we see that the matter density contrasts start out constant. This is what we would expect as the mode is frozen outside the horizon, when $k\eta << 1$. Once each mode enters the horizon $k\eta \approx 1$ causal physics begin to operate on them. Gravity then causes the matter to accumulate. For the dark matter we see that this happens simply, with the density contrast increasing monotonically until it stabilizes in the dark energy dominated era. At this time the expansion accelerates, causing the matter accumulations to stabilize at a constant value. This is also true for the large modes of baryons. For the small baryon mode however, we see an oscillation before it turns back to follow the dark matter and stabilize. This is because the smallest mode enters the horizon before recombination, meaning that the baryons are still tightly coupled to the photons. The combined baryon-photon fluid will sustain a pressure pushing against the pull of gravity, causing the density contrast to oscillate. In figure 12 we see that the velocity v_b oscillates around

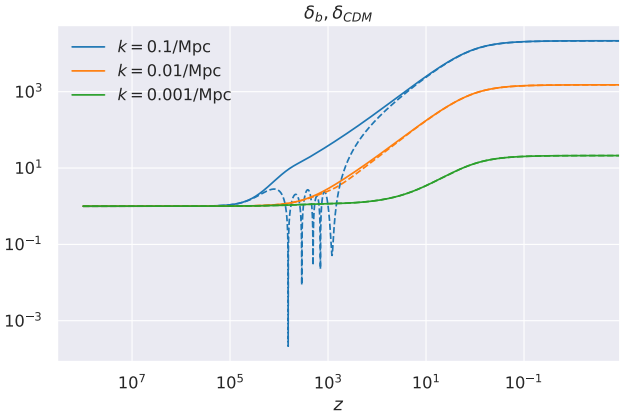

Figure 11. Evolution of the baryon and dark matter density contrasts. Note that the baryon contrasts are plotted in absolute values and are marked by dashed lines.

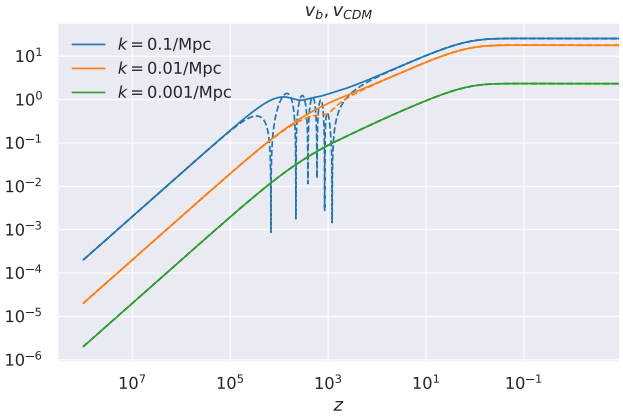

Figure 12. Evolution of the baryon and dark matter velocity perturbations. Note that the baryon perturbations are plotted in absolute values and are marked by dashed lines.

0 (we see these as pointy edges since we plot the absolute value). After the baryons decouple at recombination they fall into the gravitational wells created by the dark matter in the meantime.

In figure 13 we see that the gravitational potential falls as soon as the mode enters the horizon. As the perturbations do not grow, the potential in an expanding universe decays because of the dilution of the density. We see in particular that the smallest mode expresses the same oscillating behavior as δ_b before reaching recombination. When the dark energy dominated era is reached we see that the potential stabilizes to a constant value. In figure 14 we see that $\Psi \approx -\Phi$.

We can also see an oscillating behavior in the photon density contrast and velocity (figures 15 and 16), as we would expect if photons and baryons behave as a single fluid. For the smallest mode in discussion we see again that the oscillation begins when the mode enters

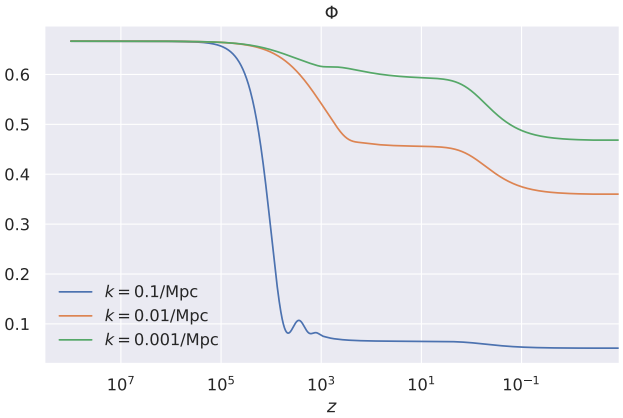

Figure 13. Evolution of the Newtonian potential.

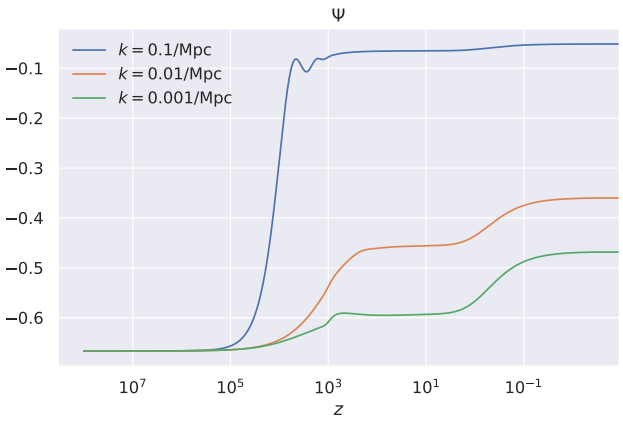

Figure 14. Evolution of Ψ.

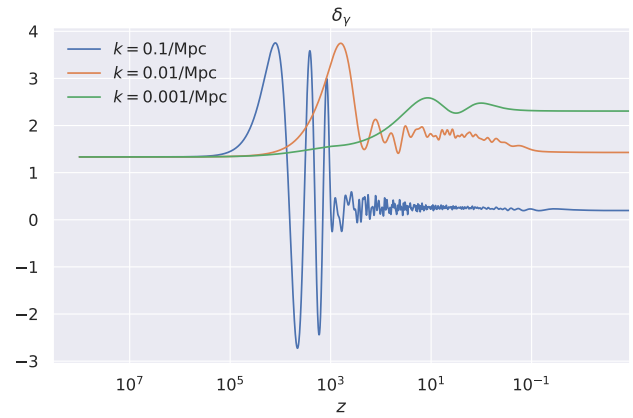

Figure 15. Evolution of the photon density contrast $\delta_\gamma = 4\Theta_0$.

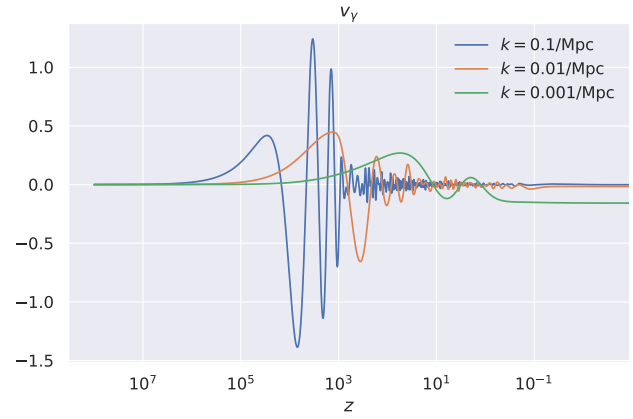

Figure 16. Evolution of the photon velocity perturbations $v_\gamma = -3\Theta_1$.

the horizon. When recombination is reached the oscillations are heavily damped before they seem to stabilize, as expected. However, we also see that the larger modes show a damped oscillating behavior after reaching the horizon.

The computed evolution of the monopole Θ_0 until recombination can very roughly be described by a driven harmonic oscillator

$$\ddot{\Theta}_0 + k^2 c_s^2 \Theta_0 = F, \tag{24}$$

where F is a driving force due to gravity and c_s is the sound speed of the baryon-photon fluid. This will come in handy in Milestone IV.

MILESTONE IV: CMB AND MATTER POWER SPECTRA

Introduction

We have now computed all the quantities we need to generate the CMB and matter power spectra. We wish to do so for values of ℓ up to ~ 2000. Since the power spectrum depends on Θ_ℓ we in principle need to calculate Θ_ℓ up to $\ell \sim 2000$. This would take a lot of computational time. There is luckily a technique that speeds up the computations significantly; line-of-sight integration. Instead of expanding the full temperature perturbation in spherical harmonics and then solving the coupled equations, one can first integrate $\dot{\Theta}$ and then expand it. Using line-of-sight integration one can therefore calculate Θ_ℓ for higher values of ℓ through simple integration. This is why we only computed up to $\ell = 7$ in the previous milestone.

Theory

The power spectrum C_ℓ is defined in terms of Θ_ℓ as

$$C_\ell \equiv \left\langle |\Theta_\ell|^2 \right\rangle. \tag{25}$$

Using line-of-sight integration we can calculate Θ_ℓ through the integral

$$\Theta_\ell(k, x=0) = \int_{-\infty}^{0} \tilde{S}(k,x) j_\ell[k(\eta_0 - \eta)] dx, \tag{26}$$

where $j_\ell(x)$ are the sperical bessel functions and the source function $\tilde{S}(k,x)$ is

$$\tilde{S}(k,x) = \tilde{g}\left[\Theta_0 + \Psi + \frac{1}{4}\Theta_2\right] + e^{-\tau}\left[\Psi' - \Phi'\right] - \frac{1}{ck}\frac{d}{dx}(\mathcal{H}\tilde{g}v_b) + \frac{3}{4c^2k^2}\frac{d}{dx}\left[\mathcal{H}\frac{d}{dx}(\mathcal{H}\tilde{g}\Theta_2)\right]. \tag{27}$$

Note that this expression for $\tilde{S}(k,x)$ assumes no polarization. If we were to include polarization we would have to change Θ_2 to $\Pi = \Theta_2 + \Theta_0^P + \Theta_2^P$.

The first term in (27) is the Sachs-Wolfe term. It describes that the observed CMB spectrum is the local monopole at the last scattering surface. There are some small corrections to this: The Ψ term takes into account that the photons lose energy as they climb out of a gravitational potential to reach us. There is also a quadrupolar correction from Θ_2 in addition to polarization if we included that.

The second term is the integrated Sachs-Wolfe term. This describes the change in the gravitational potentials as the CMB photons travel through the Universe. The third term describes the Doppler effect on the photons. The final term is the quadrupole term, which is another quadrupolar correction. For more details on line-of-sight integration see Callin [3].

Now the power spectrum C_ℓ can be calculated through

$$C_\ell = \frac{2}{\pi}\int k^2 P_{\text{primordial}}(k)\Theta_\ell^2(k)dk. \tag{28}$$

This can be simplified by noting that inflation predicts a Harrison-Zel'dovich spectrum, which means that the primordial power spectrum $P_{\text{primordial}}$ is given by

$$\frac{k^3}{2\pi^2}P_{\text{primordial}}(k) = A_s\left(\frac{k}{k_{\text{pivot}}}\right)^{n_s-1} \tag{29}$$

where k_{pivot} is some scale for which the amplitude is A_s. The final expression for the power spectrum is therefore

$$C_\ell = 4\pi\int_0^\infty A_s\left(\frac{k}{k_{\text{pivot}}}\right)^{n_s-1}\Theta_\ell^2(k)\frac{dk}{k}. \tag{30}$$

The matter power spectrum can easily be obtained from C_ℓ through

$$P(k,x) = \frac{2\pi^2}{k^3}A_s\left(\frac{k}{k_{\text{pivot}}}\right)^{n_s-1}|\Delta_M(k,x)|^2, \tag{31}$$

where

$$\Delta_M(k,x) \equiv \frac{c^2k^2\Phi(k,x)}{\frac{3}{2}\Omega_{M0}a^{-1}H_0^2}.$$

The dominant term in $\tilde{S}(k,x)$ (27) is the Sachs-Wolfe term. Recalling that the visibility function has a sharp peak at recombination, the line-of-sight integral (26) gives

$$\Theta_\ell^{\text{today}}(k) \approx [\Theta_0 + \Psi]_{\text{rec}} \cdot j_\ell(k\eta_0) \tag{32}$$

Each multipole is in other words directly related to the effective monopole at recombination. Since C_ℓ depends on Θ_ℓ^2 we get a clue of how the power spectrum will turn out based on the evolution of the monopole until recombination. As we saw in Milestone III, Θ_0 evolves as a driven harmonic oscillator (24). We also have the factor $j_\ell(k\eta_0)$, which peaks when $k\eta_0 \sim \ell$. Therefore we expect the modes k that are at peak during recombination to be mapped to peaks in the power spectrum at $\ell \sim k\eta_0$. Given figure 15 we can already say that we expect the first peak (at lowest ℓ) to come around $k \sim 0.01$/Mpc since this mode is at it first peak roughly during recombination ($z \sim 10^3$). This maps to $\ell \sim k\eta_0 \sim 10^2$.

Likewise, modes that are zero during recombination are expected to be mapped to troughs in the power spectrum. Then there will be a new peak for the mode that goes through one oscillation to reach recombination at its second peak, followed by a new trough, and so on. We therefore expect to see oscillations in the CMB spectrum for $\ell \gtrsim 10^2$.

Recall that the acoustic oscillations (24) are driven by a force F due to gravity. This force gets a constant contribution from the presence of baryons, causing the equilibrium of the oscillations to be shifted from origin. For the square of the monopole Θ_0^2, which contributes to the power spectrum, this means that the odd peaks are increased and the even peaks are decreased. This effect is called *baryon loading*.

Implementation details

The line-of-sight integral (26) was solved using the trapezoidal method. Using the resulting Θ_ℓ we computed the power spectrum (30) with the trapezoidal method for 53 values of ℓ on the interval $[2, 2000]$. We made a cubic spline of the result.

Results and Discussion

In figure 17 we see how the transfer function Θ_ℓ varies with k. We see that our expectations for the peaks were justified: They seem to map to angular scales $\ell \sim k\eta_0$. We also have a plot of the integrand Θ_ℓ^2/k of C_ℓ (30) in figure 18. Note that we have scaled it by $\ell(\ell+1)$ since that is how we will scale the plot of the power spectrum. We see that the largest contribution seems to come around $\ell \sim 200$.

In figure 19 we see the computed CMB power spectrum. For low values of $\ell \lesssim 20$ we see that our spectrum

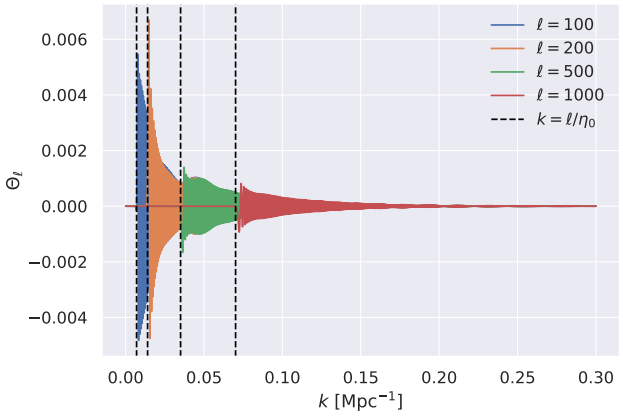

Figure 17. The transfer function.

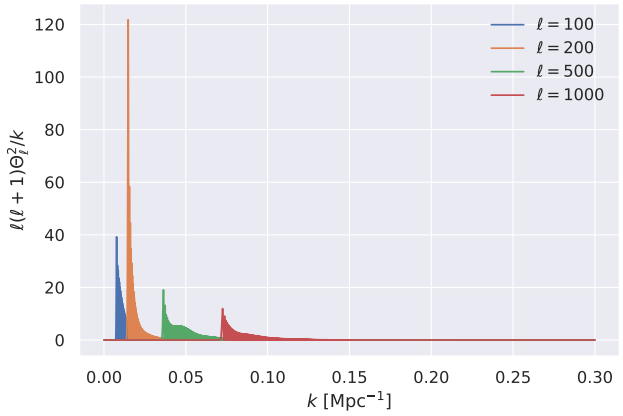

Figure 18. The integrand of C_ℓ (30).

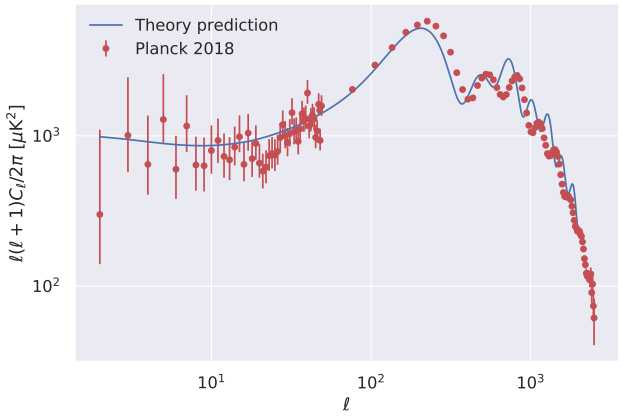

Figure 19. CMB power spectrum and Planck 2018 data [1].

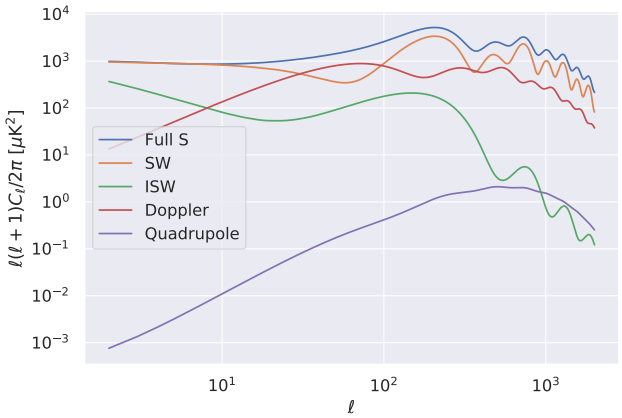

Figure 20. Contribution to CMB from each term in the source function $\tilde{S}(k, x)$: Sachs-Wolfe term, Integrated Sachs-Wolfe term, Doppler term and Quadrupole term.

follows the Sachs-Wolfe plateau. These scales correspond to the large modes that did not enter the horizon before recombination. Perturbations at these scales are essentially frozen in, subject only to energy decrease due to climbing out of the gravitational potential. The power spectrum for $\ell \lesssim 20$ is therefore directly related to the initial perturbations set up by inflation.

The first and largest peak in the power spectrum comes at $\ell \sim 200$, in agreement with our initial expectation to find it around $\ell \sim 10^2$. We see that the first peak is indeed followed by oscillations. The effect of baryon loading is also apparent; the even peaks are suppressed relative to the odd peaks, most clearly among the first three peaks.

We see that the spectrum decreases rapidly for high ℓ. To explain this, recall that we have been using the approximation that baryons and photons behave as a single fluid due to their high scattering rate. For this approximation to be perfect it would require an infinite scattering rate. In reality the photons scatter off the electrons at a finite rate in a random walk. Therefore it will move a mean distance $\lambda_D \sim 1/\sqrt{n_e \sigma_T H}$ in a Hubble time H^{-1}. Perturbations on scales smaller than λ_D are therefore washed out, which is what we see for high ℓ's.

We see that the computed spectrum is close to the observed values, with most of the spectrum within the error bars. There is however a deviation around the first peak at $l \sim 200$. We also see that the high-ℓ oscillations do not fit the observed values perfectly. Figure 20 shows how each of the source terms contribute to the power spectrum. We see that the most important term is indeed the Sachs-Wolfe-term. None of the terms show any features that are clearly wrong. It is therefore unlikely that an error in the source function is the cause of the deviation from the data.

Figure 21 shows the matter power spectrum. The dashed line marks the scale $k_{eq} = \mathcal{H}_{eq}/c$ corresponding to matter-radiation equality. The mode at k_{eq} enters the horizon at matter-radiation equality. Modes larger than this (smaller k) enters afterwards (in the matter era) and modes smaller than this enters before (in the radiation era). Since perturbations hardly grow in the radiation

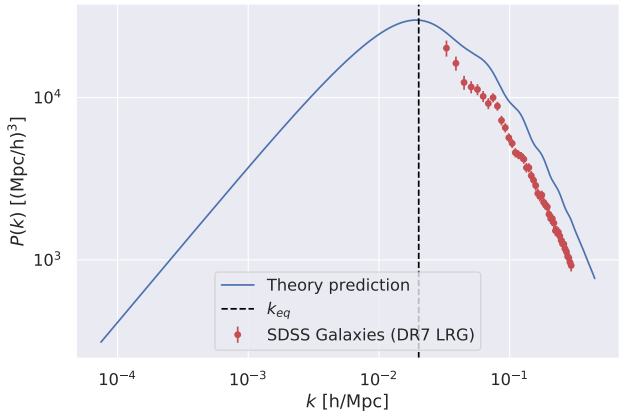

Figure 21. Matter power spectrum and SDSS Galaxies data [1].

era, the $k > k_{eq}$ spectrum is suppressed relative to the $k < k_{eq}$ spectrum. The lowest k that does not get any suppression is the one at k_{eq} since it enters exactly at matter-radiation equality, giving a peak in the spectrum. The $k > k_{eq}$ modes do grow after entry. They have however had less time to grow before the dark energy era is reached, as we saw in figure 11 of Milestone III. We therefore have that $P(k < k_{eq}) < P(k_{eq})$. The same figure reveals why we see oscillations in the power specrum for $k > k_{eq}$: It is caused by the oscillations in the baryon-photon fluid of modes entering in the radiation era (see δ_b for $k = 0.1$/Mpc).

The results for the matter power spectrum seem to make sense, but we clearly see that it does not fit the data. This is not a numerical error. It is caused by our simplification of not including neutrinos in our calculations. Including them would cause a shift in the matter-radiation equality. Given the plot we could imagine shifting the peak of the power spectrum at k_{eq} would make it fit our data. The neutrinos would also cause an additional change in our results as a source for the gravitational potential in the perturbations.

CONCLUSION

Through numerical simulation we have been able to predict CMB and matter power spectra close to agreement with observational data. In the background calculations we found the luminosity distance in close to perfect agreement with observed type 1A supernovae. Our CMB power spectrum is close to agreement with the Planck 2018 data, however with the higher multipoles in slight disagreement. The matter power spectrum turned out to be off the SDSS Galaxies data.

The disagreement with observational data was expected since we made some simplifications in our calculations. We have not considered the initial presence of neutrinos, which would change the time of matter-radiation equality. This would shift the peak of the matter power spectrum and probably make it fit the SDSS Galaxies data. It would also change our results as an additional source for the gravitational potential in the perturbations. We also did not include helium. This would change our calculations of recombination as it would add some more reactions with electrons and photons. We did not include reionization, which would add an extra peak in the visibility function in the late Universe. Polarization was not included in the calculations. This would act as a correction to the source function and also make it possible to include the effect of gravitational waves on the power spectrum. Finally, we did not include the effect of gravitational lensing on the CMB spectrum, which would act as a correction. All of these effects could be implemented and is expected to make the computed spectra fit the observed data better.

[1] Aghanim, N., Akrami, Y., Ashdown, M., Aumont, J., Baccigalupi, C., Ballardini, M., Banday, A. J., Barreiro, R. B., Bartolo, N., et al. Planck 2018 results. *Astronomy & Astrophysics 641* (Sep 2020), A6.
[2] Betoule, M., Kessler, R., Guy, J., Mosher, J., Hardin, D., Biswas, R., Astier, P., El-Hage, P., Konig, M., Kuhlmann, S., et al. Improved cosmological constraints from a joint analysis of the sdss-ii and snls supernova samples. *Astronomy & Astrophysics 568* (Aug 2014), A22.
[3] Callin, P. How to calculate the cmb spectrum.
[4] White, M. Anisotropies in the cmb.